Intensity-Modulated Micro-bend Fiber Optic Sensor for Respiratory Monitoring and Gating During MRI

Doreen Lau, Zhihao Chen, *Senior Member*, *IEEE*, Ju Teng Teo, Soon Huat Ng, Helmut Rumpel, Yong Lian, *Fellow*, *IEEE*, Hui Yang and Pin Lin Kei

***Abstract*— This paper describes a novel micro-bend Fiber Optic Sensor system (FOS) for respiratory monitoring and respiratory-gating in the MRI environment. The system enables the non-invasive real-time monitoring and measurement of breathing rate and respiratory/body movement pattern of healthy subjects inside the MRI gantry, and has potential application in respiratory-gated image acquisition based on respiratory cues. The working principle behind this sensor is based on the micro-bending effect of optical fiber on light transmission. The sensor system comprises of a 1.0 mm thin graded-index multimode optical fiber embedded plastic sensor mat, a photo-electronic transceiver and a computer with a digital signal processing (DSP) algorithm. *In vitro* testing showed that our sensor has a typical signal-to-noise ratio better than 28dB. Clinical MRI trials conducted on twenty healthy human subjects showed good and comparable breathing rate detection (with an accuracy of ±2 bpm) and respiratory-gated image quality produced using the sensor system, with reference to current predicate hospital device/system. The MRI-safe, ease of operation characteristics, low fabrication cost and extra patient comfort offered by this system suggests its good potential in replacing predicate device/system, and serve as a dual function in real-time respiratory monitoring and respiratory-gated image acquisition at the same time during MRI.**

Index Terms*— *Magnetic resonance imaging, fiber optic sensor, micro-bending, respiratory monitoring, respiratory-gating.

I. Introduction

BREATHING rate and body movement are vital physiologic parameters required for monitoring during Magnetic Resonance Imaging (MRI). The remote sensing for breathing signals of patients inside the MRI gantry is especially crucial for the monitoring of sedated, comatose and critically ill patients. Moreover, gating of MR image acquisition with respect to breathing and body movement is a key aspect in acquiring high quality MR images. Failure to control this can degrade image quality and hamper the accurate diagnosis of patients.

Conventional electronic sensors for respiratory monitoring such as the respiratory bellows are not sensitive enough to distinguish between shallow breathing and cessation of breathing [1]. The electronic sensors are also prone to electromagnetic interference (EMI) and may risk radiofrequency (RF) burns on the patients' skin due to electrical currents induced in the metal components by the changing magnetic field gradients during MRI [2-5]. In addition, physiologic sensors in recent development are mostly electronic-based e.g. piezo-electronics [6], capacitive coupled electrodes [7], electromechanical films (EMFi) [8] and magnetic impedance [9], and may not be suitable for use in the higher Tesla MRI environment. Thus, there is an increasing market demand for the development of MRI-safe respiratory monitors that can even be used in high-field MR environment.

Over the past few decades, the high sensitivity of optical fibers to external perturbations has been studied extensively for applications in the physical, biological, chemical and imaging aspects of healthcare sensing [10, 11]. Optical fibers are intrinsically safe for patient use due to their chemical inertness and non-toxicity. Their dielectric nature and small size also allow their easy installation into miniaturized devices or embedded into textile materials for sensing. In particular, they are ideal for real-time physiologic monitoring during MRI due to immunity from electromagnetic and RF interference. Many of such sensors based on the concepts of macro-bending [11], fiber Bragg-grating and optical time-domain reflectometer (OTDR) [12], fiber optic statistical mode (STM) and high order mode excitation (HOME) [13] and photo-plethysmography (PPG) [14] have been proposed for the monitoring of breathing rate and respiratory/body movement in the past, nevertheless are not feasible for industrial acceptance and clinical use due to their bulkiness, design complexity, low sensor sensitivity and high fabrication costs.

Micro-bend optical fiber sensors have been explored for physical and chemical detection of parameters such as pressure, strain, displacement, vibration, temperature,

Manuscript received November 5, 2012. This work was supported in part by the Agency for Science, Technology and Research (A*STAR) Biomedical Engineering Programme Grant 102 148 0011.

Pin Lin Kei, Doreen Lau, Helmut Rumpel and Hui Yang are with the Singapore General Hospital, Department of Radiology, Outram Road, Singapore 169608 (address correspondence to Pin Lin Kei: phone: +65 9688 2964; fax: +65 6326 5161; e-mail: kei.pin.lin@sgh.com.sg).

Zhihao Chen, Ju Teng Teo and Soon Huat Ng are with the Institute for Infocomm Research, Neural and Biomedical Technology Department, 1 Fusionopolis Way, Connexis, Singapore 138632 (phone: +65 6408 2371; e-mail: zchen@i2r.a-star.edu.sg)

Yong Lian is with the Department of Electrical and Computer Engineering, National University of Singapore, 4 Engineering Drive 3, Singapore 117576 (phone: +65-65162993; e-mail: eleliany@nus.edu.sg)

humidity, pH, etc. with good sensitivity [15-17]. These types of sensors are highly advantageous over other fiber optic sensor types for their design simplicity and inexpensive fabrication costs, and are thus suitable for both clinical and home use. We have previously presented works on micro-bend optical fiber sensor for vital signs monitoring [18-20]. Similar to other successful healthcare sensors, our micro-bend sensor technology has been commercialized for home-based healthcare sensing. However to our knowledge, no publication has reported the use of micro-bend optical fiber sensor for respiratory monitoring and gating in the MRI environment.

In this paper, we describe a novel micro-bend Fiber Optic Sensor system (FOS) for the non-invasive and real-time monitoring and recording of breathing rate for respiratory monitoring inside the MRI gantry and respiratory/body movement for respiratory-gated image acquisition during MRI. The sensing principle is based on the micro-bending effect of multimode fibers on the transmission of light along sensing fibers during breathing and body movement. The sensing system consists of a 1 mm thin optical fiber embedded plastic sensor mat, a photo-electronic transceiver and a digital signal processing (DSP) algorithm for the extraction of respiratory signals and reporting of breathing rate and respiratory/body movement of the subjects – a system that allows for the dual function of respiratory-monitoring and respiratory-gated image acquisition to be performed together at the same time during the MR imaging session. Data from our clinical validation of the FOS were presented to demonstrate its feasibility of operation during MRI.

II. Materials And Methods

A. Concept, Design, and Fabrication of FOS

The theory of optical fibers for the micro-bend sensing of vital signs has been proven both theoretically and experimentally in previous studies [15-17].

The FOS comprises of a sensor mat embedded with multimode optical fiber, a photo-electronic transceiver and a computer with a DSP algorithm as illustrated in Fig. 1. The optical fiber used to construct the sensor is a graded-index multimode fiber with a core diameter of 100 µm (OFS Fitel LLC, Georgia, USA). The mat was constructed to a dimension of 30 x 45 cm for placement on the MRI bed (under the diaphragm region of the patient for respiratory sensing).

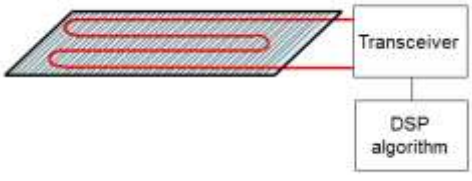

Fig. 1. Schematic diagram of FOS. The FOS comprises of a sensor mat embedded with multimode optical fiber, a photo-electronic transceiver and a computer with a digital signal processing (DSP) algorithm.

The sensor design is based on micro-bending effect created through a "sandwich" micro-bender structure (Fig. 2). Under mechanical perturbations such as periodic movement (respiratory chest and body movement), the deformer plates squeeze the optical fiber and induce a series of micro-bends along the fiber axis.

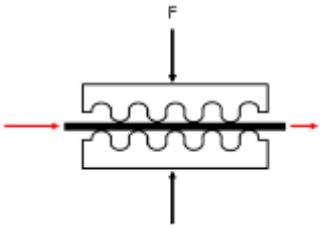

Fig. 2. A micro-bend multimode fiber under deformation by mechanical force *F* exerted during breathing motion.

The deformer plates apply a pressure ΔF to the bent fiber causing the amplitude of the fiber deformation X to change by an amount ΔX. The transmission coefficient T for light traveling along the bent fiber is changed by an amount ΔT so that [21]:

$$\Delta T = \left(\frac{\Delta T}{\Delta X}\right)\Delta F\left(k + \frac{AY}{l}\right)^{-1} \quad (1)$$

where k is the force constant of the bent fiber, A is the cross sectional area, Y is the Young's modulus, and l is the length of the deformer spacers. The graph in Fig. 3 shows a typical relationship between the normalized sensor output and the force exerted.

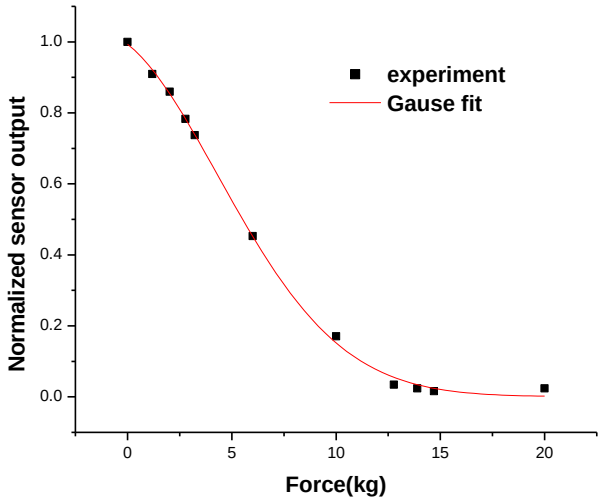

Fig. 3. Relationship between force exerted on the sensor mat and normalized output of the sensor.

This type of sensor's sensitivity is force dependent. As can be seen from Fig.3, the sensor output approaches zero as the force is larger than 12kg. Although the sensor's output is force dependent, our sensor works fine for most subjects because only small area of the body is contacted with the sensor mat and the force exerted is still below the threshold of the force.

Micro-bending causes light coupling from core guided modes into radiation modes, resulting in irreversible light loss and

decreased (modulated) light intensity detected by the transceiver. By measuring the modulation in light intensity, the breathing rate and respiratory/body movement information of the patient within a specific time can be obtained through the DSP algorithm.

Maximum micro-bend sensitivity was achieved by proper construction of the optical fiber such that the spatial frequency Λ of the micro-benders satisfies the approximate relationship [21]:

$$\Lambda = \frac{2\pi a}{\sqrt{2\Delta}} \quad (2)$$

where a is the fiber core radius and Δ is the relative refractive index difference.

The interrogation unit for FOS is in the form of a transceiver that comprises of a LED light source operating at 1310 nm, a light detector with a detection range of 1100-1650 nm, a micro-processor and other circuits, and a USB interface for connection to a computer running the DSP algorithm. The output of the transceiver is digital signal sampled at 10Hz. Peak detection was performed in the time domain for calculation of the breathing rate. To eliminate the noises, the input signal is first filtered by a bandpass filter with cut-off frequencies at 0.05-0.5 Hz. This extracts the distinct feature of breathing rate. The workflow in signal processing is shown in Fig. 4. Fig.5 is a typical frequency spectrum of the breathing signal. Fig.6 shows a typical breathing waveform where the signal to noise ratio is better than 28dB. The breathing rate and respiratory/body movement pattern were then displayed on the algorithm GUI for respiratory monitoring and respiratory-gated image acquisition.

NI LabVIEW (National Instruments Corporation, Texas, USA) programming language was used to design the application software (DSP algorithm). The software operates on a two-level platform – 1) Data acquisition and recording; and 2) Data analysis of the recorded data. Fig. 7 shows the GUI display of the software.

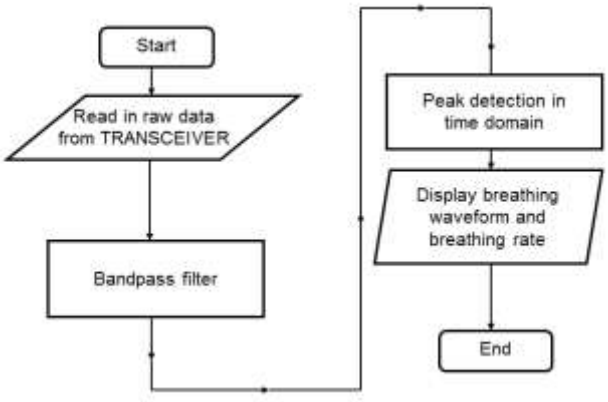

Fig. 4. Workflow in processing a modulated signal using FOS.

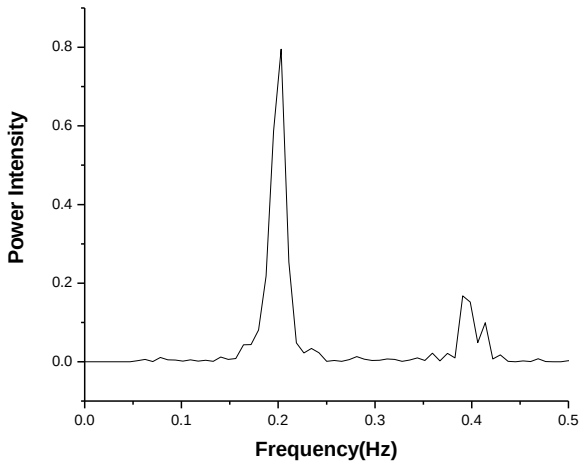

Fig. 5. Frequency spectrum showing a measured breathing signal in the range 0.05-0.5 Hz.

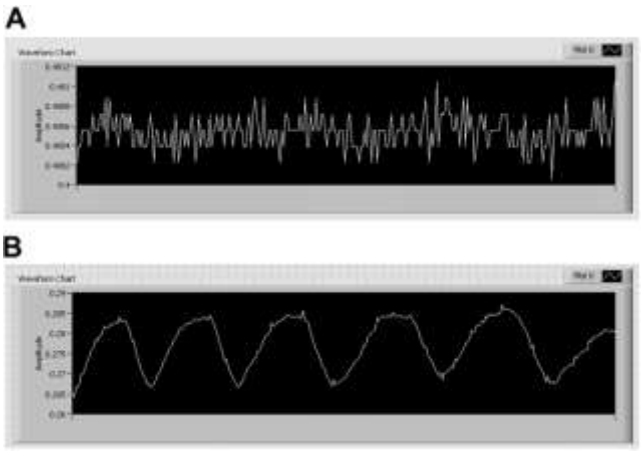

Fig. 6. The top waveform **A** shows the noise floor (0.0008 v) of the transceiver and the bottom waveform **B** shows the breathing signal detected (0.02 v). The signal-to-noise ratio is better than 28 dB.

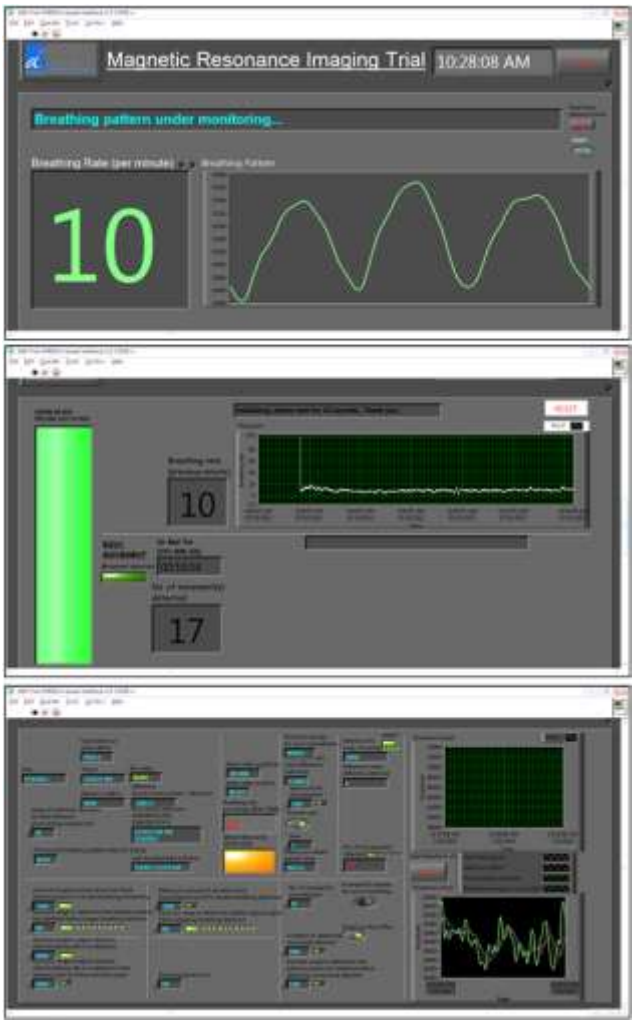

Fig. 7. GUI of the DSP algorithm. It displayed the breathing rate and breathing and body movement pattern on the main screen for respiratory monitoring and respiratory-gated image acquisition.

B. Clinical validation of the sensor

A comparative study was carried out to prospectively evaluate FOS for its dual function in breathing rate detection and respiratory-gated image acquisition during MRI with predicate hospital device/system.

An institutional review board approved clinical trial was conducted and informed consent was obtained from all subjects prior to imaging. Twenty healthy subjects were enrolled into the study. Each subject underwent T2-weighted half-Fourier single-shot turbo spin-echo (HASTE) MRI of the liver with simultaneous breathing rate monitoring on a 1.5 Tesla (T) MR scanner (MAGNETOM Avanto, Siemens Medical Solutions, Erlangen, Germany) using a phased array coil. Fig. 8 shows the experimental setup of the sensor system in the MRI room for the clinical trial.

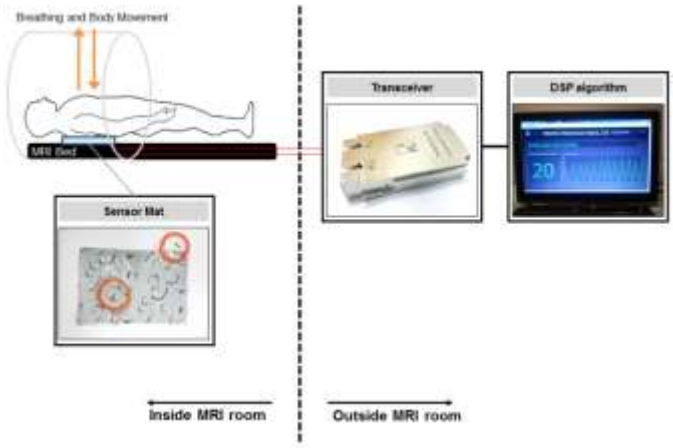

Fig. 8. Experimental setup of FOS system for breathing rate and respiratory/body movement monitoring during MRI examination.

The subjects were positioned supine, with their diaphragm region resting on the sensor mat for respiratory monitoring inside the MRI gantry during the MRI procedure. The respiratory bellows (Physiological Measurement Unit, Siemens Medical Solutions, Erlangen, Germany) is a conventional pneumatic pressure transducer that has been routinely used in hospitals for respiratory monitoring during MRI. The bellows was strapped with a belt around the subjects' lower chest to measure chest wall expansion with respiration, according to routine clinical practice. As the manufacturer's respiratory measurement system does not allow for extraction of the respiratory waveform produced by the respiratory bellows for comparison to FOS, a single investigator observed and recorded down the breathing rate detected individually by FOS and the respiratory bellows every 5 minutes interval during the 30-minute MR imaging session. The average breathing rate detected for each subject using FOS during the entire imaging duration was then computed for statistical comparison to the respiratory bellows.

For the MR imaging, single slice liver images were obtained at the portal vein confluence with 2 signal averages using three different image acquisition techniques; namely respiratory-gated image acquisition by observing FOS chest/body movement waveform pattern, the predicate two-dimensional prospective acquisition correction (2D PACE) Navigator echo respiratory-gating technique and non-respiratory-gated image acquisition (Fig. 9). The liver was selected as the imaging position as the organ is located just below the diaphragm, thus will be subjected to respiratory movement. The predicate Navigator echo software allows for the synchronization of respiratory movement with imaging by monitoring the diaphragm motion in a region-of-interest on the right hemi-diaphragm and allows image acquisition only when the diaphragm is positioned within a small predetermined acceptance window.

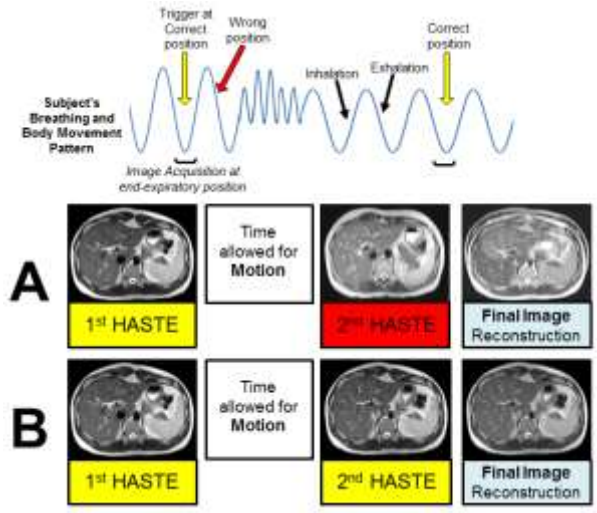

Fig. 9. Single slice HASTE liver images were obtained at the portal vein confluence with 2 HASTE signal averages for all three imaging techniques: respiratory-gating using FOS breathing and respiratory/body movement pattern as respiratory cues for image acquisition, respiratory-gating using Navigator echoes and non-respiratory-gated image acquisition. To obtain FOS-gated images, time was allowed for respiratory motion (breathing and body movement) between each triggering for HASTE signal acquisition at the end-expiratory position. The final reconstructed image is the sum of the two signals (1st and 2nd HASTE) for all three imaging techniques. The wrong trigger for 2nd HASTE by the radiographer will produce final reconstructed FOS images affected by motion blurring (Scenario **A**), while the correct triggering of 2nd HASTE at the end-expiratory position when observing the respiratory/body movement waveform on the DSP algorithm will produce FOS images that are clear and of good quality (Scenario **B**).

C. MR Image Analysis

Blinded quantitative and qualitative image quality assessments were performed on all liver MR images using an open-source software package (OsiriX version 4.0). The mean signal intensities (SI) of the liver, the spleen and the background noise in the axial images were measured using an operator-defined region-of-interest (ROI) analysis. To minimize errors, the ROIs placed on all images were of identical shapes and sizes and were taken at an average of three measurements (Fig. 10). ROI signal intensities measurements of the liver and the spleen were conducted on each image in the same anatomical location in areas devoid of large vascular structures. The standard deviation of background noise signal (SD_B) was measured in the phase-encoding direction by placing the ROI just ventral to the right anterior abdominal wall outside the body, encompassing any image artifacts that may be present. The image liver signal-to-noise ratio (SNR) and liver and spleen contrast-to-noise ratio (CNR) were calculated based on standard formulae (3) and (4):

$$\text{SNR of the Liver} = SI_{Liver} / SD_B \quad (3)$$

$$\text{CNR of the Liver and the Spleen} = |SI_{Liver} - SI_{Spleen}| / SD_B \quad (4)$$

Fig. 10. Region-of-interest (ROI) quantitative analysis of the liver MRI images.

For qualitative assessment of the images, image sets (in both axial and coronal planes) acquired using all three image acquisition techniques were presented in a blinded and random fashion and examined side-by-side by a radiologist. The images were graded on a modified 5-point image scoring scale [23] and compared for the overall image quality, the clarity of liver and hepatobiliary features and the presence of artifacts. The overall image quality was evaluated using the following scale: 1 = unreadable, 2 = poor quality, 3 = satisfactory quality, 4 = good quality and 5 = excellent quality. The clarity of liver and hepatobiliary anatomic features (liver edges, biliary tree, hepatic veins and portal veins) was assessed using the following scale: 1 = unreadable, 2 = severe blur, 3 = moderate blur, 4 = mild blur and 5 = sharp. Last but not least, the following image scoring scale was used to evaluate the presence of image artifacts: 1 = unreadable study, 2 = severe artifacts, 3 = moderate artifacts, 4 = mild artifacts and 5 = no artifacts.

D. Statistical Analysis

All statistical analyses were performed using SPSS Statistics 17.0 (SPSS Inc, Chicago, IL). The breathing rate detected by FOS was compared to the respiratory bellows using a paired *t* test ($p < 0.05$). The liver SNR and liver-to-spleen CNR were compared for the images acquired using the three different image acquisition techniques using a repeated measures ANOVA pairwise comparison of variance ($p < 0.05$). The qualitative image scores were evaluated using the Friedman test with post-hoc Wilcoxon signed-rank analysis for image quality difference between the FOS-gated images and the Navigator-acquired images ($p < 0.05$).

III. Results

There were twenty healthy adult subjects enrolled for the study (10 males and 10 females) of ages 24 – 61 years old. Their weights ranged between 44.3 – 75.2 kg, and were within the healthy Body Mass Index (BMI) range 18.7 – 26.6 kg/m^2. Among the twenty subjects, one subject declared a past medical history of childhood asthma; another subject had a history of hyperthyroidism (a metabolism-related disease) but currently well controlled. One subject declared to have an underlying medical history of G6PD deficiency, and one subject had a smoking history of 30 years. The remaining 16 subjects declared no past medical history at the point of MRI examination. The age range, gender, weight/BMI range and

medical history of the study group were representative of the regular patient base examined in hospitals.

The mean breathing rate detected by FOS and the predicate respiratory bellows were similar with an accuracy of ± 2 breath rate per minute ($p > 0.05$) (Fig. 11 and Table 1). The healthy subjects displayed different breathing rates (8-22 breath-rate per minute) and breathing pattern of various forms (slow to fast; shallow to deep breathing) during the MRI examination (Fig. 12) and displayed as sinusoid waveform on the computer screen (Fig. 7).

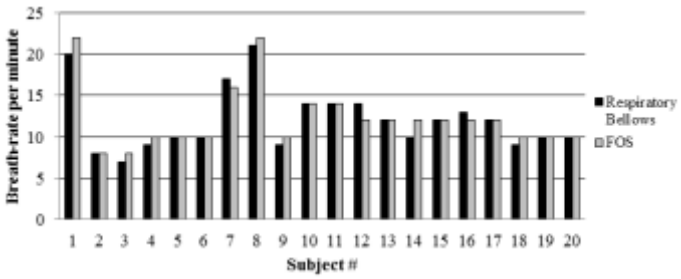

Fig. 11. Breathing rate detected and recorded for all 20 healthy subjects by each respiratory monitoring device during 1.5T MRI.

Respiratory monitoring device	Respiratory Bellows	FOS
Breath-rate per minute	12.05 ± 3.78	12.30 ± 3.85

Table 1. A comparison of breathing rate detected by the fiber optic sensor system and the respiratory bellows during MRI on a 1.5T MRI scanner. No significant difference in breathing rate detected was seen between FOS and the respiratory bellows ($p = 0.262 > 0.05$).

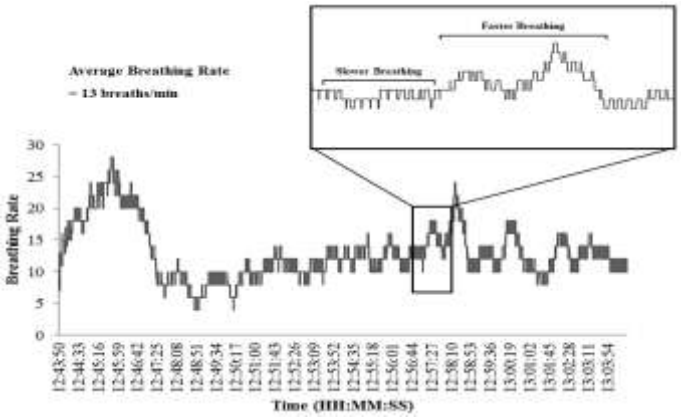

Fig. 12. A 20 min recording of the breathing rate and breathing waveform of a 26 year old male healthy subject during respiratory-gated image acquisition inside the MRI gantry of a 1.5T MRI scanner. FOS is sensitive in detecting variations in breathing rates of all healthy subjects when they are undergoing imaging inside the MRI gantry.

Pairwise comparison for rating of image quality obtained showed no significant difference in the liver SNR and liver-to-spleen CNR between the FOS-gated images and the Navigator-acquired images ($p > 0.05$) (Table 2). Wilcoxon signed-rank analysis of the qualitative image scores on the 5-point image scoring scale to evaluate the diagnostic quality of the MR images were significantly different between the FOS-gated and Navigator-acquired images for all 3 image scoring criteria; namely the overall image quality ($p < 0.05$), the clarity of liver and hepatobiliary anatomic features ($p < 0.001$) and presence of image artifacts ($p < 0.05$). Nevertheless, FOS-gated images were generally graded good to excellent for the overall image quality; the liver and hepatobiliary anatomical features were relatively sharp with mild blurriness and image artifacts due to motion effects were mild to absent (mean score 4 and above for all criteria) (Table 3). In a number of occasion (in about 40%), FOS-gated images were graded an image score of 5 (unpublished data) with comparable or better image quality to than images produced using Navigator-acquired scans. In comparison to the non-gated images, motion-induced artifacts in the form of image ghosting in the phase-encoding direction, blurring and signal voids were rarely seen in images acquired using FOS respiratory-gating. Fig. 13 shows the liver MR images obtained from 5 healthy subjects at 1.5T MRI. The liver edges were clearly outlined, and liver vascular structures such as the portal veins and even smaller vessels such as the hepatic veins were relatively well-depicted on the FOS-gated liver images.

Quantitative Image Measurements	Non-gated	FOS	Navigator Echoes
Liver SNR	72.55 ± 19.01	78.70 ± 15.50	78.72 ± 18.62
Liver-to-Spleen CNR	61.55 ± 33.69	94.27 ± 17.58	95.72 ± 26.30

Table 2. Quantitative evaluation of Liver Signal-to-Noise Ratio (SNR) and Liver-to-Spleen Contrast-to-Noise Ratio (CNR) for image quality of liver MR images obtained at 1.5T using the three different imaging techniques. No significant difference in image SNR ($p = 1.000 > 0.05$) and CNR ($p = 1.000 > 0.05$) was seen between FOS-gated images and Navigator-gated images.

Image Scoring	Non-gated	FOS	Navigator Echoes
Overall image quality	2.57 ± 0.84	4.25 ± 0.63	4.60 ± 0.55
Clarity of anatomic features	2.78 ± 0.83	4.22 ± 0.67	4.59 ± 0.54
Liver edge	2.70 ± 0.72	4.17 ± 0.71	4.60 ± 0.55
Portal veins	2.85 ± 0.89	4.23 ± 0.70	4.60 ± 0.55
Biliary tree	2.78 ± 0.83	4.20 ± 0.65	4.58 ± 0.55
Hepatic veins	2.80 ± 0.88	4.30 ± 0.65	4.60 ± 0.55
Artifacts	2.75 ± 0.84	4.23 ± 0.66	4.65 ± 0.53

Table 3. Qualitative analysis of the MR image quality of images obtained at 1.5T on a 5-point image scoring scale. There were significant differences in the overall image quality ($p = 0.023 < 0.05$), clarity of liver and hepatobiliary anatomic features ($p = 0.000 < 0.001$) and presence of artifacts ($p = 0.006 < 0.05$) between FOS-gated images and Navigator-acquired images. Neverthless, all FOS-gated images were generally graded good to excellent (mean score 4 and above) on the 5-point image scoring scale for all three image assessment criteria.

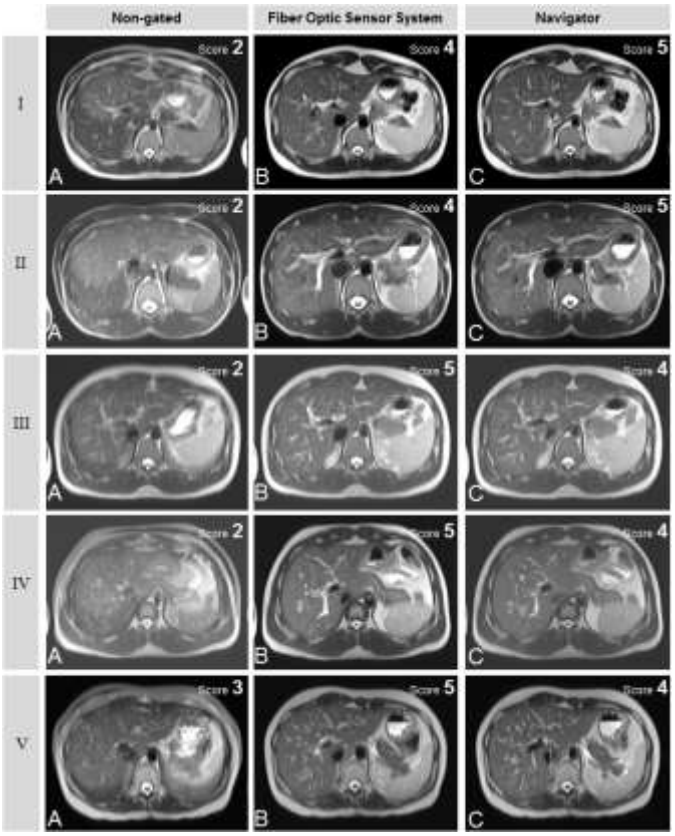

Fig. 13. A comparison of liver MRI images obtained at 1.5T from 5 healthy subjects (Subject ***I*** -***V***) using FOS for respiratory-gated image acquisition (***B***) with Navigator echoes based respiratory-gated images (***C***) and images obtained without any respiratory-gating (i.e. without motion compensation / non-gated) (***A***). Motion artifacts were mild or absent and anatomic structures such as the portal veins can clearly be seen in the FOS-gated images. FOS-gated images were generally graded score 4 and above for good to excellent overall image quality. In some instances, FOS-gated images even scored the highest for overall image quality among all three imaging techniques (see subjects ***III***-***V***). The presence of the fiber optic sensor mat inside the MRI gantry during imaging did not lead to any obvious image distortions in all images.

IV. Discussion

A growing patient population and world-wide government drive towards preventive therapies motivate an increasingly demanding market for minimally invasive engineering solutions, which includes the use of innovative materials like optical fibers in medical device development.

Optical sensing for patient physiologic monitoring is coming-of-age and revolutionary for medicine, ever since these hair-thin strands of glass or plastic fibers were first successfully implemented for endoscopic imaging in the 1960s [10, 11]. Nevertheless, despite the many physical and chemical advantages optical fiber sensors offer over conventional electronic sensors, market penetration has been slow due to several reasons; Optical fiber sensors and their interrogation units developed in the past were of high cost. Their complex system design and poor end-user interface also pose challenges for regulatory approval and industry acceptance [11-14, 26], especially with regard to physiologic sensing in a busy hospital setting like the MRI room.

In this study, a novel micro-bend optical sensing system (FOS) has been developed for the real-time monitoring of patients' breathing rate and respiratory/body movement inside the MRI gantry. Breathing information transmitted in the form of modulated light intensity was largely not affected by the RF pulses and magnetic field gradients emitted by the 1.5T MR scanner. FOS was able to detect and record the breathing rate of the subjects in a satisfactory way as compared to the predicate respiratory bellows, without any significant over- or under-estimation of the breathing rate. Although technical difficulties have limited the direct comparison of FOS respiratory waveform to the respiratory bellows, our prior field trial conducted during polysomnography (PSG) in the sleep laboratory showed significant correlation in breathing rate measurement between FOS and conventional thoracic belt (Pearson's coefficient, r = 0.865) [22]. Analysis using Bland-Altman had showed only a small mean difference (< 1 bpm) i.e. 0.12 bpm (95% confidence interval [0.44, 0.68]) in breathing rate detection between the two respiratory monitoring devices [22]. FOS was also able to produce respiratory waveforms of resemblance to waveforms generated using the thoracic belt (Fig. 14).

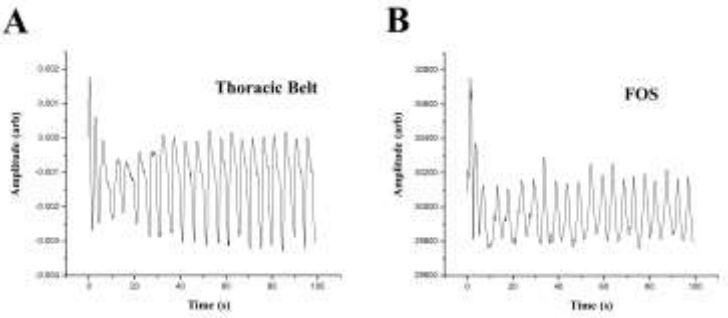

Fig. 14. A comparison between the respiratory waveforms measured by FOS and the conventional thoracic belt during PSG.

Our clinical study has also demonstrated the possibility in using respiratory cues (end-expiratory) of FOS for respiratory-gating during MRI. Unlike the Navigator, FOS allows for a real-time monitoring of the subjects' respiratory/body movement without the assumption of a regular breathing motion, and can possibly be applied on patients with respiratory problems exhibiting diaphragm drifts that can prolong Navigator-acquired scans [24, 25]. As expected, image distortion was not seen in the images obtained with the presence of the sensor mat in the 1.5T MR scanner as optical fibers materials are immune from EMI, unlike certain conventional electronic sensors [2, 3]. The liver MR images obtained using FOS for respiratory-gating were of good diagnostic quality. There was no significant reduction in MR image signal intensities and contrast in the phase-encoding direction of the images, which would have otherwise been seen in images affected by motion effects. Although the FOS-gated images were of generally good to excellent score for the overall image quality, their image scores were lower as compared to the Navigator-acquired images (p < 0.05). This was possibly due to inter-operator differences during the manual triggering of scan using FOS respiratory-gating by

different radiographers (five different radiographers with varying years of experience in MR imaging), in contrast to the system automated Navigator-acquired scans. As a result, the image scores of FOS-gated images performed slightly poorer as compared to the Navigator-acquired scans. This can potentially be resolved by integrating FOS with the MR imaging system for fully-automated scans, so as to minimize any human or slice-misregistration errors for a more direct and justified comparison between the two respiratory-gating techniques.

Besides serving its dual function in respiratory monitoring and respiratory-gating, FOS also offers several advantages over predicate respiratory bellows in terms of its safety and good operation characteristics. Being entirely constructed of non-ferromagnetic materials, the sensor mat is not only MRI-safe, but also versatile for use in different MRI environment, even with future high-field MR scanners. We have conducted a preliminary trial on 10 healthy subjects using a 3T MR scanner (MAGENTOM Skyra, Siemens Medical Solutions, Erlangen, Germany). Similar to this clinical study done at 1.5T MRI, our further evaluation of FOS in a higher magnetic field (3T) environment also showed comparable breathing rate detected between the same FOS prototype and the predicate respiratory bellows. Images obtained using FOS-gating in 3T MR environment were of good and comparable SNR and CNR to the Navigator-acquired images, and were scored good to excellent on the 5-point image scoring scale by the same radiologist. No obvious image distortions were seen in the images obtained at 3T with the presence of FOS sensor mat inside the MRI gantry. This has further verified the device's safely for use in different MRI environment (see Supplementary).

Besides its MR compatibility, the design of FOS is simple yet robust, and the cost of fabrication is low. Operating FOS is easy and no extra preparation time is needed to strap the sensor to the healthy subjects' bodies for respiratory monitoring. The sole requirement for the sensor mat placement on the MRI bed for monitoring eliminate the hassles associated with extra preparation time needed to strap conventional electronic sensors to the patients' bodies for monitoring and incidents of cable or electrodes dropping off in the middle of the MRI examination. There was also no complaint of discomfort from the healthy subjects as the sensor mat is as thin as a bed sheet and does not require skin-contact to serve its dual functions in respiratory monitoring and respiratory gating.

V. Conclusion

In this paper, we investigated FOS for its real-time monitoring of patients' respiratory/body movement inside the MRI gantry. Clinical MRI trials conducted on twenty healthy human subjects demonstrated feasibility in using FOS for both respiratory monitoring and respiratory-gating during MRI i.e. the sensing system was able to detect a comparable breathing rate to the respiratory bellows and produce liver MRI images of good and comparable image quality to the Navigator-acquired scans. With further evaluation and improvement to the device, the FOS has the potential to replace predicate systems to serve a dual function in respiratory monitoring and respiratory-gating at the same time during MRI.

Besides being MRI-safe, operating FOS is easy and only requires "plug and play" for use. The thin sensor mat also offers extra patient comfort while delivering its functions. Last but not least, the design simplicity, robustness and non-invasiveness of FOS should enable its low cost production and easier regulatory approval and industry acceptance.

Remark: Part of this work was presented as a "Late-Breaking Research" paper at the 34th Annual International Conference of the IEEE Engineering in Medicine and Biology Society, EMBC'12, San Diego, California, USA, 28 August – 1 September 2012.

Acknowledgment

This work was funded by the Agency for Science, Technology and Research (A*STAR) Biomedical Engineering Programme Grant 102 148 0011. We wish to thank the Institute of Infocomm Research, Singapore General Hospital and the National University of Singapore for their support in this study.

References

[1] D. Varshneya, and J. L. Maida, "Fibre optic monitor using interferometry for detecting vital signs of a patient", *US patent* No. 6,498,652 B1, 2002.

[2] F. G. Shellock, "Monitoring during MRI. An evaluation of the effect of high-field MRI on various patient monitors", *Med. Electron.*, vol. 17, no. 4, pp. 93-97.

[3] B. A. Holshouser, D. B. Hinshaw, and F. G. Shellock, Sedation, anesthesia and physiologic monitoring during MR imaging: evaluation of procedures and equipment", *J. Magn. Reson. Imaging*, vol. 3, pp. 553-558, 1993.

[4] R. R. Price, "The AAPM/RSNA physics tutorial for residents. MR imaging safety considerations", *Radiographics*, vol. 19, no. 6, pp. 1641-1651, 1999.

[5] H. Kugel, C. Bremer, M. Püschel M., R. Fischbach, H. Lenzen, B. Tombach, H. van Aken, and W. Heindel, "Hazardous situation in the MR bore: induction in ECG leads causes fire", *Eur. Radiol.*, vol. 13, no. 4, pp. 690-694, 2003.

[6] G. Roopa, K. Rajanna, and M. M. Nayak, "Non-invasive human breath sensor", *IEEE Sensors J.*, pp. 1788-1791, 2011.

[7] T. H. Kang, C. Merritt, B. Karaguzel, J. Wilson, P. Franzon, B. Pourdeyhimi, E. Grant, and T. Nagle, "Sensors on textile substrates for home-based healthcare monitoring", *1st Transdisciplinary Conference on Distributed Diagnosis and Home Heathcare 2006*, pp. 5-7, 2006.

[8] S. Rajala, and J. Lekkala, "Film-type sensor materials PVDF and EMFi in measurement of cardiorespiratory signals – a review", *IEEE Sensors J.*, vol. 12, no. 3, pp. 439-446, 2012.

[9] M. Steffen, A. Aleksandrowicz, and S. Leonhardt, "Mobile noncontact monitoring of heart and lung activity", *IEEE Trans. Biomed. Circuits Sys.*, vol. 1, no. 4, pp. 250-257, 2007.

[10] A. G. Mignani, and F. Baldini, "Fibre-optic sensors in health care", *Phys. Med. Biol.*, vol. 42, pp. 967-979, 1997.

[11] A. Grillet, D. Kinet, J. Witt, M. Schukar, K. Krebber, F. Pirotte, and A. Depre, "Optical fibre sensors embedded into medical textiles for healthcare monitoring", *IEEE Sensors J.*, vol. 8, no. 7, pp. 1215-1222, 2008.

[12] L. Dzuida, F. W. Skibniewski, M. Krej, and J. Lewandowski, "Monitoring respiration and caridac activity using Fiber Bragg Grating-based sensor", *IEEE Trans. Biomed. Eng.*, vol. 59, no. 7, pp. 1934-1942, 2012.

[13] W. B. Spillman, M. Mayer, J. Bennett, J. Gong, K. E. Meissner, B. Davis, R. O. Claus, A. A. Muelenaer, and X. Xu, "A smart bed for non-intrusive monitoring of patient physiological factors", *Meas. Sci. Technol.*, vol. 15, pp. 1614-1620, 2004.

[14] L. G. Lindberg, H. Ugnell, and P. A. Oberg, "Monitoring of respiratory and heart rates using a fibre-optic sensor", *Med. Biol. Eng. Comput.*, vol. 30, pp. 533-537, 1992.

[15] J. W. Berthold, "Historical review of microbend fibre-optic sensors," *J. Lightwave Technol.*, vol. 13, pp. 1193, 1995.

[16] S. Thomas Lee, B. Aneeshkumar, P. Radhakrishnan, C. P. G. Vallabhan, and, V. P. N. Nampoori, "A microbend fibre optic pH sensor", *Optics Communications*, 205, pp. 253-256, 2002.

[17] M. Linec, and D. Donlagic, "A plastic optical fiber microbend sensor used as low cost anti-squeeze detector", *IEEE Sensors J.*, vol. 7, pp. 1262-1267, 2007.

[18] Z. H. Chen, J. T. Teo, and X. F. Yang, "In-bed fibre optic breathing and movement sensor for non-intrusive monitoring", *Optical fibers and sensors for medical diagnostics and treatment applications IX, edited by Israel Gannot, Proc. of SPIE*, vol. 7173, pp. 71730P, 2009.

[19] Z. H. Chen, J. T. Teo, S. H. Ng, and H. Q. Yim, "Smart pillow for heart rate monitoring using a fiber optic sensor", *Optical fibers and sensors for medical diagnostics and treatment applications IX, edited by Israel Gannot, Proc. of SPIE*, vol. 7894, pp. 789402, 2011.

[20] Z. H. Chen, J. T. Teo, S. H. Ng, and X. F. Yang, "Portable fiber optic ballistocardiogram sensor for home use", *Proc. of SPIE*, vol. 8218, pp. 82180x, 2012.

[21] N. Lagakos, J. H. Cole and J. A. Bucaro, "Microbend fiber-optic sensor", *Appl. Opt.*, vol. 26, no. 11, pp. 2181-2180, 1987.

[22] Mark Tong, Tai Bee Choo, and Ai Ping Chua, "Evaluation Report: Comparing the use of I2R's SleepMonitor I with conventional thoracic belts in the assessment of respiratory effort, during polysomnography (PSG)", 5 Nov 2012.

[23] J. Zhang, G. M. Israel, E. M. Hecht, G. A. Krinsky, J. S. Babb, and V. S. Lee, "Isotropic 3D T2-weighted MR cholangiopancreatography with parallel imaging: feasibility study", *Am. J. Roentgenology*, vol. 187, pp. 1564-1570, 2006.

[24] A. M. Taylor, P. Jhooti, F. Wiesmann, J. Keegan, D. N. Firmin, and D. J. Pennell, "MR navigator-echo monitoring of temporal changes in diaphragm position: Implications for MR coronary angiography", *J. Magn. Reson. Imaging*, vol. 7, no. 4, pp. 629-636, 1997.

[25] J. Keegan, P. Gatehouse, G. Yang, and D. Firmin, "Coronary artery motion with the respiratory cucle during breath-holding and fre-breathing: Implications for slice-followed coronary artery imaging", *Magn. Reson. Med.*, vol. 47, no. 3, pp. 476-481, 2002.

[26] È. Pinet, "Medical applications: Saving lives", *Nature Photonics, Industry Perspective: Technology Focus*, vol. 2, pp. 150-152, 2008.

SUPPLEMENTARY

A preliminary study was conducted on a 3T MRI scanner (MAGNETOM Skyra, Siemens Medical Solutions, Erlangen, Germany) on 10 healthy subjects for further evaluation of FOS performance and safety at a higher magnetic strength environment. Results are as shown in Table S1-3 and Fig. S1-2.

Respiratory monitoring device	Respiratory bellows	FOS
Breath-rate per minute	11.90 ± 2.23	11.40 ± 1.89

Table S1. Respiratory monitoring of the 10 healthy subjects inside the MRI gantry of a 3T MRI scanner. Similar to the study conducted at 1.5T, no significant difference in breathing rate detected was seen between FOS and the respiratory bellows ($p = 0.096 > 0.05$).

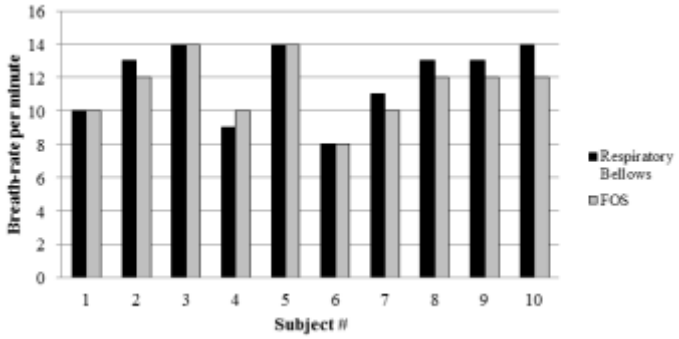

Fig. S1. Breathing rate detected and recorded for all 10 healthy subjects by each respiratory monitoring device during 3T MRI.

Quantitative Image Measurements	Non-gated	FOS	Navigator Echoes
Liver SNR	72.55 ± 19.01	78.70 ± 15.50	78.72 ± 18.62
Liver-to-Spleen CNR	61.55 ± 33.69	94.27 ± 17.58	95.72 ± 26.30

Table S2. Liver Images obtained at 3T using the three same different imaging techniques (as at 1.5T) were quantitatively evaluated for the Liver Signal-to-Noise Ratio (SNR) and Liver-to-Spleen Contrast-to-Noise Ratio (CNR). No significant difference in image SNR ($p = 0.083 > 0.05$) and CNR ($p = 0.610 > 0.05$) was seen between FOS-gated images and Navigator-gated images.

Image Scoring	Non-gated	FOS	Navigator Echoes
Overall image quality	2.57 ± 0.84	4.25 ± 0.63	4.60 ± 0.55
Clarity of anatomic features	2.78 ± 0.83	4.22 ± 0.67	4.59 ± 0.54
Liver edge	2.70 ± 0.72	4.17 ± 0.71	4.60 ± 0.55
Portal veins	2.85 ± 0.89	4.23 ± 0.70	4.60 ± 0.55
Biliary tree	2.78 ± 0.83	4.20 ± 0.65	4.58 ± 0.55
Hepatic veins	2.80 ± 0.88	4.30 ± 0.65	4.60 ± 0.55
Artifacts	2.75 ± 0.84	4.23 ± 0.66	4.65 ± 0.53

Table S3. Qualitative analysis of the MR image quality of the same set of images obtained at 3T on a 5-point image scoring scale. Due to inter-operator differences, the image scores of FOS-gated images obtained using manual triggering of scans were significantly lower than the automated Navigator-acquired images for the overall image quality ($p = 0.033 < 0.05$), clarity of liver and hepatobiliary anatomic features ($p = 0.000 < 0.001$) and presence of artifacts ($p = 0.018 < 0.05$). Neverthless, all FOS-gated images were generally graded good to excellent (mean score 4 and above) on the 5-point image scoring scale for all three image assessment criteria.

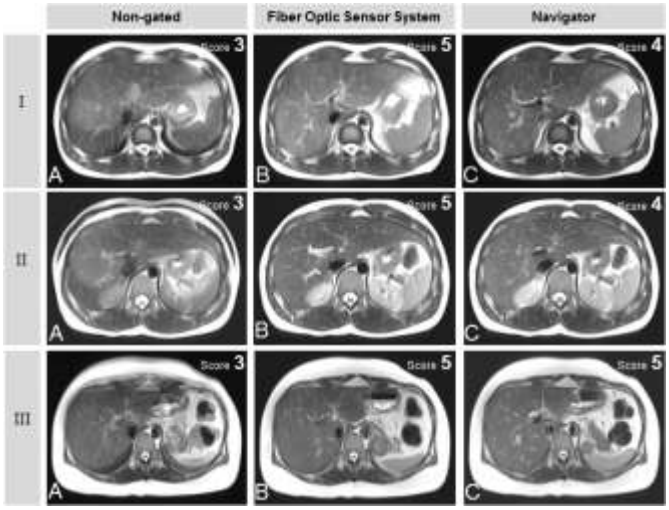

Fig. S2. A comparison of 3T MRI liver images obtained from 3 healthy subjects (Subject ***I*** -***III***) using FOS for respiratory-gated image acquisition (***B***) with Navigator echoes based respiratory-gated images (***C***) and images obtained without any respiratory-gating (i.e. without motion compensation / non-gated) (***A***). Motion artifacts were mild or absent and anatomic structures such as the portal veins can clearly be seen in the FOS-gated images obtained at 3T and the images were generally graded score 4 and above for good to excellent overall image quality. In some instances, FOS-gated images were even given the highest score of 5 for the overall image quality (see subjects ***III***). The presence of the fiber optic sensor mat inside the MRI gantry during imaging at a higher magnetic field strength (3T) did not lead to any obvious image distortions in all images.